

# Ellipticity and prolaticity of the initial gravitational-shear field at the position of density maxima

C. Angrick\*

Universität Heidelberg, Zentrum für Astronomie, Institut für Theoretische Astrophysik, Philosophenweg 12, 69120 Heidelberg, Germany

*A&A manuscript, version May 3, 2013*

## ABSTRACT

Dark-matter haloes are supposed to form at the positions of maxima in the initial matter density field. The gravitational-shear field's ellipticity and prolaticity that serve as input for the ellipsoidal-collapse model, however, are derived from a distribution that does not take the additional maximum constraint into account. In this article, I quantify the variations of the most probable and the expected values of the ellipticity and the prolaticity when considering this additional constraint. Based on the statistics of Gaussian random fields, it is possible to set up a joint distribution for the eigenvalues of the gravitational-shear tensor and the matter density that incorporates the maximum constraint by invoking a vanishing first derivative and a negative definite second derivative of the density field into the calculation. Both the most probable and the expected value of the ellipticity calculated under the assumption of a density maximum are about 1 – 8 % lower compared to the standard distribution used in the literature in the density range relevant for cosmological structure formation. Additionally, the analogous quantities for the prolaticity do not vanish but acquire slight positive values in the range of  $10^{-7}$  to  $10^{-2}$ . For large overdensities, the predictions from both distributions converge. The non-vanishing prolaticity may have consequences for the ellipsoidal-collapse model especially when the linear model for the external shear is used.

**Key words.** cosmology: theory – methods: analytical – cosmology: dark matter – cosmology: cosmological parameters – galaxies: clusters: general

## 1. Introduction

Galaxies and galaxy clusters as collapsed objects are supposed to form from peaks in the initial matter density field. After an overdense patch has decoupled from the Hubble expansion, the extent of this patch is supposed to reach a maximum value, then to shrink again until the collapse stops when the structure reaches virial equilibrium. Analytical models for this evolution include the spherical-collapse model (e.g. Wang & Steinhardt 1998; Pace et al. 2010) and the ellipsoidal-collapse model (e.g. Bartelmann et al. 1993; Eisenstein & Loeb 1995; Bond & Myers 1996).

From the theory of inflation, the density field is supposed to be a random field whose non-Gaussianity is small (Planck Collaboration XXIV 2013). Since also derivatives and integrals of Gaussian random fields are again Gaussian, a multivariate Gaussian random field can be used to derive the initial number density of peaks in the density field as a function of peak height by applying respective constraints to the density field's first and second derivatives (Bardeen et al. 1986).

Not only can the density field be described as a Gaussian random field, but through Poisson's equation, also the gravitational field has to follow a Gaussian distribution and therefore also the eigenvalues of the gravitational-shear tensor can be derived from the statistics of Gaussian random fields (Zel'dovich 1970; Doroshkevich 1970). These eigenvalues can be combined to define the ellipticity and the prolaticity of the gravitational-shear field whose distribution for a given value of the overdensity can be derived by transformation of variables (Sheth et al. 2001) and either their most probable or their expected values are

important ingredients for the ellipsoidal-collapse model by Bond & Myers (1996).

However, this distribution does not take into account that haloes should form at *maxima* in the density field, but rather yields the probability density for ellipticity and prolaticity for *any* overdensity irrespective if it is taken at a maximum or not. Recently, attempts have been made to take the maximum constraint into account when calculating the gravitational-shear tensor's constrained eigenvalues (Rossi 2012) as well as the constrained ellipticity and prolaticity from them (Rossi 2013) by extending the formalism of Doroshkevich (1970) and Sheth et al. (2001) in the way to also include the density's Hessian. One crucial condition for a maximum, namely the vanishing first derivative of the density, however, is not taken into account. Additionally, it does not seem possible in the framework of Rossi (2012, 2013) to derive the distribution for the unconstrained ellipticity and prolaticity necessary for the ellipsoidal-collapse model since the gravitational-shear tensor and Hessian of the density cannot be diagonalised simultaneously.

In this article, I will show how the distribution of the gravitational shear's ellipticity and prolaticity at the position of density maxima can be derived from the statistics of Gaussian random fields by accounting for both the vanishing first derivative of the density and the constraint that the density's Hessian has to be negative definite. In § 2, I give a short introduction to Gaussian random fields and show step-by-step how the targeted distribution can be calculated invoking the technique to derive number densities from multivariate Gaussians of the relevant quantities based on Bardeen et al. (1986) and how the constraint for the density's Hessian can be properly considered without diagonalisation. In § 3, I compare the results from the distribution includ-

\* e-mail: angrick@uni-heidelberg.de

ing the maximum constraint to the one by Sheth et al. (2001) that does not take it into account. Finally, I summarise the main results of this article in § 4 and briefly hint at implications for the ellipsoidal-collapse model by Bond & Myers (1996).

## 2. The conditional distribution for ellipticity and prolativity

In this section, I derive the conditional probability for the ellipticity and the prolativity of the gravitational shear from the statistics of Gaussian random fields. First, I give a brief overview over the theoretical background of Gaussian random fields based on Bardeen et al. (1986) (see also Angrick & Bartelmann 2009 for further information). Hence I also adopt  $F(\mathbf{r})$  for the random field and  $\eta(\mathbf{r}) = \nabla F(\mathbf{r})$  and  $\zeta_{ij}(\mathbf{r}) = \partial_i \partial_j F(\mathbf{r})$  for its first and second derivatives, respectively.

### 2.1. Theoretical background

An  $n$ -dimensional random field  $F(\mathbf{r})$  assigns a set of random numbers to each point in  $n$ -dimensional space. A joint probability function can be declared for  $m$  arbitrary points  $\mathbf{r}_j$  as the probability that the field  $F$ , considered at the points  $\mathbf{r}_j$ , has values between  $F(\mathbf{r}_j)$  and  $F(\mathbf{r}_j) + dF(\mathbf{r}_j)$  with  $1 \leq j \leq m$ .

A Gaussian random field is a field whose joint probability functions are multivariate Gaussians. Let  $y_i$  with  $1 \leq i \leq p$  be a set of Gaussian random variables with means  $\langle y_i \rangle$  and  $\Delta y_i \equiv y_i - \langle y_i \rangle$ . The covariance matrix  $\mathbf{M}$  has the elements  $M_{ij} \equiv \langle \Delta y_i \Delta y_j \rangle$ , and the joint probability function of the Gaussian random variables is

$$p(y_1, \dots, y_p) dy_1 \dots dy_p = \frac{1}{\sqrt{(2\pi)^p \det \mathbf{M}}} e^{-Q} dy_1 \dots dy_p \quad (1)$$

with the quadratic form

$$Q \equiv \frac{1}{2} \sum_{i,j=1}^p \Delta y_i (\mathbf{M}^{-1})_{ij} \Delta y_j. \quad (2)$$

In the following, I will only consider fields on the 3-dimensional Euclidean space with coordinates  $\mathbf{r} = (x_1, x_2, x_3)^T$ . A homogeneous Gaussian random field with zero mean is fully characterised by its two-point correlation function  $\xi_F(\mathbf{r}_1, \mathbf{r}_2) = \xi_F(|\mathbf{r}_1 - \mathbf{r}_2|) \equiv \langle F(\mathbf{r}_1) F(\mathbf{r}_2) \rangle$  or equivalently its Fourier transform, the power spectrum  $P_F(k)$ . Its spectral moments are defined by

$$\sigma_j^2 \equiv \int_0^\infty \frac{dk}{2\pi^2} P_F(k) k^{2j+2} \hat{W}_R^2(k), \quad (3)$$

where  $\hat{W}_R(k)$  is the Fourier transform of the filter function  $W_R(\mathbf{r})$ , and  $R$  is its filter size. In the following, I adopt Gaussian filtering, hence  $W_R(\mathbf{r}) = \exp[-|\mathbf{r}|^2/(2R^2)]$  and  $\hat{W}(k) = \exp(-R^2 k^2/2)$ . The zeroth-order spectral moment  $\sigma_0^2$  is the power spectrum's variance.

It is possible to scale the field  $F$  as well as its derivatives with corresponding spectral moments so that they become dimensionless. I will denote these reduced fields with a tilde, e.g.  $\tilde{F} = F/\sigma_0$ ,  $\tilde{\eta} = \eta/\sigma_1$ , and  $\tilde{\zeta} = \zeta/\sigma_2$ . A quantity that will be used more often in the next sections is a special combination of the first three spectral moments,  $\gamma \equiv \sigma_1^2/(\sigma_0 \sigma_2)$ .

The elements  $\varphi_{ij}$  of the gravitational-shear tensor  $\varphi$  (Zel'dovich 1970) contain the scaled second derivatives of the gravitational potential  $\Phi$ ,

$$\varphi_{ij} = \frac{1}{4\pi G \rho_b} \frac{\partial^2 \Phi}{\partial x_i \partial x_j}, \quad (4)$$

where  $G$  is Newton's constant and  $\rho_b$  the background matter density, so that  $\text{tr } \varphi = \delta$  by Poisson's equation. Here,  $\delta$  is the dimensionless overdensity defined by  $\delta \equiv (\rho - \rho_b)/\rho_b$ . I will denote the eigenvalues of  $\varphi$  with  $\lambda_i$ , where  $1 \leq i \leq 3$ . The ellipticity  $e$  and the prolativity  $p$  are combinations of these eigenvalues,

$$e = \frac{\lambda_1 - \lambda_3}{2\delta}, \quad p = \frac{\lambda_1 - 2\lambda_2 + \lambda_3}{2\delta} \quad \text{with} \quad \delta = \lambda_1 + \lambda_2 + \lambda_3. \quad (5)$$

Ordering the eigenvalues in the way  $\lambda_1 \geq \lambda_2 \geq \lambda_3$ , as it is commonly done in the literature, imposes the constraints  $e \geq 0$  and  $-e \leq p \leq e$  for  $\delta \geq 0$ . Since a spherical configuration has  $\lambda_1 = \lambda_2 = \lambda_3$ , this is equivalent to  $e = p = 0$ . While the ellipticity measures the anisotropy in the  $x_1$ - $x_3$ -plane, the prolativity quantifies the shape perpendicular to it: if  $p < 0$ , the configuration is *prolate*, for  $p > 0$  it is *oblate*. Note that ellipticity and prolativity are defined on the linear density field and should not be confused with the shape of the final halo!

Following Bardeen et al. (1986), the conditional probability for the random variables  $e$  and  $p$  given a maximum of reduced height  $\tilde{\delta}$  can be expressed as

$$P(e, p | \tilde{\delta}, \text{max}) = \frac{\int_{n.d.} d^6 \tilde{\zeta} |\det \tilde{\zeta}| P(e, p, \tilde{\delta}, \tilde{\eta} = \mathbf{0}, \tilde{\zeta})}{\int_{n.d.} d^6 \tilde{\zeta} |\det \tilde{\zeta}| P(\tilde{\delta}, \tilde{\eta} = \mathbf{0}, \tilde{\zeta})}, \quad (6)$$

where here and in the following,  $\tilde{\eta}$  is the reduced first derivative of  $\tilde{\delta}$  and  $\tilde{\zeta}$  is the corresponding Hessian, which has only six independent components since it is symmetric. Note that only those subvolumes contribute to the integral for which  $\tilde{\zeta}$  is negative definite (indicated by *n.d.*), i.e. its three eigenvalues are negative. How this can be properly taken into account, I will discuss in Sect. 2.3.

### 2.2. The joint probability of relevant quantities

To calculate  $P(e, p | \tilde{\delta}, \text{max})$ , I shall start with establishing the 15-dimensional joint probability of reduced variables  $P(\tilde{\varphi}, \tilde{\eta}, \tilde{\zeta}) d^6 \tilde{\varphi} d^3 \tilde{\eta} d^6 \tilde{\zeta}$  to evaluate the numerator of Eq. (6).

The correlation matrix  $\mathbf{M}$  incorporates all auto- and cross-correlations of the various random variables. These are

$$\begin{aligned} \langle \tilde{\varphi}_{ij} \tilde{\varphi}_{kl} \rangle &= \frac{1}{15} \kappa_{ijkl}, & \langle \tilde{\eta}_i \tilde{\eta}_j \rangle &= \frac{1}{3} \delta_{ij}, \\ \langle \tilde{\zeta}_{ij} \tilde{\zeta}_{kl} \rangle &= \frac{1}{15} \kappa_{ijkl}, & \langle \tilde{\varphi}_{ij} \tilde{\zeta}_{kl} \rangle &= -\frac{\gamma}{15} \kappa_{ijkl}, \end{aligned} \quad (7)$$

where  $\delta_{ij}$  is the Kronecker symbol and the quantity  $\kappa_{ijkl}$  is a combination of Kronecker symbols given by  $\kappa_{ijkl} \equiv \delta_{ij} \delta_{kl} + \delta_{ik} \delta_{jl} + \delta_{il} \delta_{jk}$ . All other correlations apart from those listed above vanish (cf. also Bardeen et al. 1986; Rossi 2012). Defining the vector of random variables  $\mathbf{y} = (\tilde{\varphi}_{11}, \tilde{\varphi}_{22}, \tilde{\varphi}_{33}, \tilde{\varphi}_{12}, \tilde{\varphi}_{13}, \tilde{\varphi}_{23}, \tilde{\eta}_1, \tilde{\eta}_2, \tilde{\eta}_3, \tilde{\zeta}_{11}, \tilde{\zeta}_{22}, \tilde{\zeta}_{33}, \tilde{\zeta}_{12}, \tilde{\zeta}_{13}, \tilde{\zeta}_{23})^T$ , the correlation matrix  $\mathbf{M}$  looks like

$$\mathbf{M} = \frac{1}{15} \begin{pmatrix} \mathbf{A} & \mathbf{0} & \mathbf{0} & -\gamma \cdot \mathbf{A} & \mathbf{0} \\ \mathbf{0} & \mathbf{1} & \mathbf{0} & \mathbf{0} & -\gamma \cdot \mathbf{1} \\ \mathbf{0} & \mathbf{0} & 5 \cdot \mathbf{1} & \mathbf{0} & \mathbf{0} \\ -\gamma \cdot \mathbf{A} & \mathbf{0} & \mathbf{0} & \mathbf{A} & \mathbf{0} \\ \mathbf{0} & -\gamma \cdot \mathbf{1} & \mathbf{0} & \mathbf{0} & \mathbf{1} \end{pmatrix}, \quad (8)$$

where the different submatrices are given by

$$\mathbf{A} = \begin{pmatrix} 3 & 1 & 1 \\ 1 & 3 & 1 \\ 1 & 1 & 3 \end{pmatrix}, \quad \mathbf{1} = \begin{pmatrix} 1 & 0 & 0 \\ 0 & 1 & 0 \\ 0 & 0 & 1 \end{pmatrix}, \quad \mathbf{0} = \begin{pmatrix} 0 & 0 & 0 \\ 0 & 0 & 0 \\ 0 & 0 & 0 \end{pmatrix}. \quad (9)$$

The determinant of  $\mathbf{M}$  is

$$\det \mathbf{M} = \frac{2^4(1-\gamma^2)^6}{3^{15} \cdot 5^{10}}, \quad (10)$$

and the inverse of  $\mathbf{M}$  is

$$\mathbf{M}^{-1} = \frac{3}{2(1-\gamma^2)} \begin{pmatrix} \mathbf{C} & \mathbf{0} & \mathbf{0} & \gamma \cdot \mathbf{C} & \mathbf{0} \\ \mathbf{0} & 10 \cdot \mathbb{1} & \mathbf{0} & \mathbf{0} & 10\gamma \cdot \mathbb{1} \\ \mathbf{0} & \mathbf{0} & 2(1-\gamma^2) \cdot \mathbb{1} & \mathbf{0} & \mathbf{0} \\ \gamma \cdot \mathbf{C} & \mathbf{0} & \mathbf{0} & \mathbf{C} & \mathbf{0} \\ \mathbf{0} & 10\gamma \cdot \mathbb{1} & \mathbf{0} & \mathbf{0} & 10 \cdot \mathbb{1} \end{pmatrix}, \quad (11)$$

where  $\mathbb{1}$  and  $\mathbf{0}$  are defined as above and

$$\mathbf{C} = \begin{pmatrix} 4 & -1 & -1 \\ -1 & 4 & -1 \\ -1 & -1 & 4 \end{pmatrix}. \quad (12)$$

Rotating the coordinate system such that  $\tilde{\varphi}$  becomes diagonal and assuming that the eigenvalues are ordered like  $\tilde{\lambda}_1 \geq \tilde{\lambda}_2 \geq \tilde{\lambda}_3$ , [Bardeen et al. \(1986\)](#) showed that the volume element  $d^6\tilde{\varphi}$  can be written as

$$d^6\tilde{\varphi} = 2\pi^2(\tilde{\lambda}_1 - \tilde{\lambda}_2)(\tilde{\lambda}_1 - \tilde{\lambda}_3)(\tilde{\lambda}_2 - \tilde{\lambda}_3) d\tilde{\lambda}_1 d\tilde{\lambda}_2 d\tilde{\lambda}_3. \quad (13)$$

Note that the two matrices  $\tilde{\varphi}$  and  $\tilde{\zeta}$  do not commute and hence cannot be diagonalised simultaneously. Therefore, I still have to keep the off-diagonal elements of  $\tilde{\zeta}$  in the following calculation, whereas  $\tilde{\varphi}_{12} = \tilde{\varphi}_{13} = \tilde{\varphi}_{23} = 0$  and  $\tilde{\varphi}_{ii} = \tilde{\lambda}_i$  after the diagonalisation.

Switching from the eigenvalues to the new variables  $\tilde{\delta}$ ,  $e$ , and  $p$ , the Jacobi determinant of the transformation introduces an additional factor so that

$$d\tilde{\lambda}_1 d\tilde{\lambda}_2 d\tilde{\lambda}_3 = \frac{2}{3} \tilde{\delta}^2 d\tilde{\delta} de dp. \quad (14)$$

Altogether, the integrand in the numerator of Eq. (6) can be written as

$$P(e, p, \tilde{\delta}, \tilde{\eta} = \mathbf{0}, \tilde{\zeta}) |\det \tilde{\zeta}| = \left(\frac{3}{2}\right)^{13/2} \frac{5^5}{\pi^{11/2}(1-\gamma^2)^3} e(e^2-p^2) \tilde{\delta}^5 \exp \left\{ \frac{1}{2(\gamma^2-1)} \left[ 3(2\tilde{\delta}^2 - 5\tilde{\Delta}) + 2\gamma\tilde{\delta}\tilde{\zeta}_\zeta(1+15ee_\zeta+5pp_\zeta) + \tilde{\delta}^2(1+15e^2+5p^2) \right] \right\} |\det \tilde{\zeta}|, \quad (15)$$

where I have introduced the abbreviations

$$\begin{aligned} \tilde{\Delta} &\equiv \tilde{\zeta}_{11}\tilde{\zeta}_{22} + \tilde{\zeta}_{11}\tilde{\zeta}_{33} + \tilde{\zeta}_{22}\tilde{\zeta}_{33} - \tilde{\zeta}_{12}^2 - \tilde{\zeta}_{13}^2 - \tilde{\zeta}_{23}^2, \\ \tilde{\delta}_\zeta &\equiv \tilde{\zeta}_{11} + \tilde{\zeta}_{22} + \tilde{\zeta}_{33}, \quad e_\zeta \equiv \frac{\tilde{\zeta}_{11} - \tilde{\zeta}_{33}}{2\tilde{\delta}_\zeta}, \quad p_\zeta \equiv \frac{\tilde{\zeta}_{11} - 2\tilde{\zeta}_{22} + \tilde{\zeta}_{33}}{2\tilde{\delta}_\zeta}, \end{aligned} \quad (16)$$

and with

$$\det \tilde{\zeta} = \tilde{\zeta}_{11}\tilde{\zeta}_{22}\tilde{\zeta}_{33} + 2\tilde{\zeta}_{12}\tilde{\zeta}_{13}\tilde{\zeta}_{23} - \tilde{\zeta}_{11}\tilde{\zeta}_{23}^2 - \tilde{\zeta}_{22}\tilde{\zeta}_{13}^2 - \tilde{\zeta}_{33}\tilde{\zeta}_{12}^2. \quad (17)$$

### 2.3. Sylvester's criterion

To evaluate the numerator of Eq. (6), I have to integrate over those parts of the volume spanned by the matrix elements of  $\tilde{\zeta}$  for which the latter is negative definite. This can be achieved by taking into account the following criterion. A Hermitian matrix is positive definite if and only if all its leading principal minors are positive, where the  $i$ -th leading principal minor is the determinant of its upper left  $i \times i$  sub-matrix. This is known as *Sylvester's criterion*.

Since the negative of a positive definite and Hermitian matrix is negative definite, this implies that all odd principal minors have to be negative and all even principal minors have to be positive. Technically, when integrating Eq. (15) numerically over the various matrix elements, I multiply it by a function  $f(\tilde{\zeta})$  defined as

$$f(\tilde{\zeta}) \equiv \begin{cases} 1 & \text{if } \tilde{\zeta}_{11} < 0 \wedge \begin{vmatrix} \tilde{\zeta}_{11} & \tilde{\zeta}_{12} \\ \tilde{\zeta}_{12} & \tilde{\zeta}_{22} \end{vmatrix} > 0 \wedge \begin{vmatrix} \tilde{\zeta}_{11} & \tilde{\zeta}_{12} & \tilde{\zeta}_{13} \\ \tilde{\zeta}_{12} & \tilde{\zeta}_{22} & \tilde{\zeta}_{23} \\ \tilde{\zeta}_{13} & \tilde{\zeta}_{23} & \tilde{\zeta}_{33} \end{vmatrix} < 0, \\ 0 & \text{else,} \end{cases} \quad (18)$$

and integrate over all six elements from  $-\infty$  to  $\infty$ .

### 2.4. The number density of maxima in the density field

Analogous to the way I have derived Eq. (15), it is possible to derive the joint probability  $P(\tilde{\delta}, \tilde{\eta}, \tilde{\zeta}) d\tilde{\delta} d^3\tilde{\eta} d^6\tilde{\zeta}$ . A similar and more detailed description of the various steps can be found in [Angrick & Bartelmann \(2009\)](#), where I have derived the number density of minima in the gravitational potential. Rotating the coordinate system such that  $\tilde{\zeta}$  becomes diagonal and transforming to the variables  $\tilde{\delta}_\zeta$ ,  $e_\zeta$ , and  $p_\zeta$  introduced in Eq. (16), which are combinations of the eigenvalues  $\tilde{\lambda}_{\zeta,i}$  of  $\tilde{\zeta}$  after the rotation, the integrand in the denominator of Eq. (6) can be written as

$$P(\tilde{\delta}, \tilde{\eta} = \mathbf{0}, \tilde{\zeta}) |\det \tilde{\zeta}| = \frac{25\sqrt{15}}{8\pi^3 \sqrt{1-\gamma^2}} e_\zeta(e_\zeta^2 - p_\zeta^2) \left[ (1+p_\zeta)^2 - 9e_\zeta^2 \right] (2p_\zeta - 1) |\tilde{\delta}_\zeta^8 \times \exp \left[ \frac{(\tilde{\delta}^2 + \tilde{\delta}_\zeta^2 + 2\gamma\tilde{\delta}\tilde{\delta}_\zeta + (1-\gamma^2)(15e_\zeta^2 + 5p_\zeta)\tilde{\delta}_\zeta^2)}{2(\gamma^2-1)} \right], \quad (19)$$

where I have ordered the eigenvalues of  $\tilde{\zeta}$  like  $\tilde{\lambda}_{\zeta,1} \geq \tilde{\lambda}_{\zeta,2} \geq \tilde{\lambda}_{\zeta,3}$ . To evaluate the denominator of Eq. (6), I have to integrate over the eigenvalues  $\tilde{\lambda}_{\zeta,i}$  from  $-\infty$  to 0, or, since I have transformed to the new variables  $\tilde{\delta}_\zeta$ ,  $e_\zeta$ , and  $p_\zeta$ , integrate over them in the proper range. The condition  $0 \geq \tilde{\lambda}_{\zeta,1} \geq \tilde{\lambda}_{\zeta,2} \geq \tilde{\lambda}_{\zeta,3}$  translated to the new variables reads

$$\tilde{\delta}_\zeta \leq 0 \wedge \left[ \left( -\frac{1}{2} \leq e_\zeta \leq -\frac{1}{4} \wedge -1 - 3e_\zeta \leq p_\zeta \leq -e_\zeta \right) \vee \left( -\frac{1}{4} < e_\zeta \leq 0 \wedge e_\zeta \leq p_\zeta \leq -e_\zeta \right) \right]. \quad (20)$$

Note that the variables  $\tilde{\delta}_\zeta$  and  $e_\zeta$  are negative in contrast to the analogous variables  $\tilde{\delta}$  and  $e$  for the gravitational-shear tensor.

It turns out that the integrations over  $e_\zeta$  and  $p_\zeta$  can be done analytically, while the integration over  $\tilde{\delta}_\zeta$  has to be done numerically. The denominator of Eq. (6) is equal to the number density

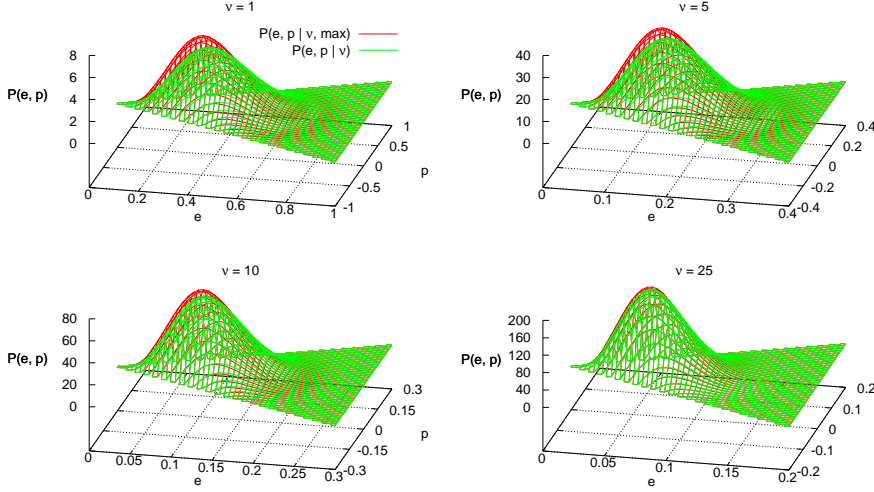


**Fig. 1.** The distributions  $P(e, p | v, \max)$  based on Eq. (6) and  $P(e, p | v)$  based on Eq. (24) for four different values of  $v = \delta_c^2 / \sigma_0^2$ .

of maxima  $n_{\max}(\tilde{\delta})$  of the reduced density field  $\tilde{\delta}$  if multiplied by a factor  $\sigma_2^3 / \sigma_1^3$ . The latter can be written as

$$n_{\max}(\tilde{\delta}) = \frac{\sigma_2^3}{\sigma_1^3} \int_{-\infty}^0 d\tilde{\delta}_\zeta \frac{u}{1200\pi^3 \sqrt{3(1-\gamma^2)}} (\sqrt{5}v + 25\sqrt{2\pi}w) \quad (21)$$

with

$$u = \exp \left[ \frac{\tilde{\delta}^2 + 2\gamma \tilde{\delta} \tilde{\delta}_\zeta + \tilde{\delta}_\zeta^2 (6 - 5\gamma^2)}{2(\gamma^2 - 1)} \right],$$

$$v = 10\tilde{\delta}_\zeta^2 - 32 + (155\tilde{\delta}_\zeta^2 + 32) \exp \left( \frac{15\tilde{\delta}_\zeta^2}{8} \right),$$

$$w = \tilde{\delta}_\zeta (\tilde{\delta}_\zeta^2 - 3) \exp \left( \frac{5\tilde{\delta}_\zeta^2}{2} \right) \left[ \operatorname{erf} \left( \frac{1}{2} \sqrt{\frac{5}{2}} \tilde{\delta}_\zeta \right) + \operatorname{erf} \left( \sqrt{\frac{5}{2}} \tilde{\delta}_\zeta \right) \right]. \quad (22)$$

Now I have all the ingredients to express the probability to find the ellipticity  $e$  and the prolativity  $p$  of the gravitational-shear field in the range  $[e, e + de]$  and  $[p, p + dp]$  given a density peak of height  $\delta$ . To summarise, after scaling it to the reduced density  $\tilde{\delta} = \delta / \sigma_0$ , it is given by the ratio (6), where the numerator is expressed by Eq. (15) together with Eq. (16), and the denominator by Eqs. (21) and (22) except the factor  $\sigma_2^3 / \sigma_1^3$ . Equation (18) offers a nice way to take into account the constraint that Eq. (15) has to be integrated only over those subvolumes for which the matrix  $\tilde{\zeta}$  is negative definite.

### 2.5. Comparison to the ansatz of Rossi

Rossi (2012) derives a conditional probability for the reduced shear tensor  $\tilde{\varphi}$  given positive definite Hessian  $\tilde{\zeta}$  (see his Eqs. (18) and (19)). In the language of this paper, his probability looks like

$$P(\tilde{\varphi} | \tilde{\zeta}, p.d.) = \frac{\int_{p.d.} d^6 \tilde{\zeta} P(\tilde{\zeta}) P(\tilde{\varphi} | \tilde{\zeta})}{\int_{p.d.} d^6 \tilde{\zeta} P(\tilde{\zeta})} \text{ with } P(\tilde{\varphi} | \tilde{\zeta}) = \frac{P(\tilde{\varphi}, \tilde{\zeta})}{P(\tilde{\zeta})}, \quad (23)$$

where *p.d.* indicates integration over the subvolume for which  $\tilde{\zeta}$  is positive definite. The reason for this complicated way of writing is the aim to diagonalise both the conditional matrix  $\tilde{\varphi} | \tilde{\zeta}$

and the matrix  $\tilde{\zeta}$  to use their eigenvalues in the further calculation. Additionally, both  $P(\tilde{\varphi} | \tilde{\zeta})$  and  $P(\tilde{\zeta})$  can be written as an expression analogous to the distribution of the gravitational-shear tensor's eigenvalues derived by Doroshkevich (1970).

However, it is not possible to diagonalise both matrices  $\tilde{\varphi} | \tilde{\zeta}$  and  $\tilde{\zeta}$  simultaneously since the commutator of the two does not vanish. Hence, the aim of Rossi (2013) that this ansatz can be used to determine the probability  $P(e, p | \delta, \max)$  from Eq. (23), implying that the eigenvalues of both the former matrices can be used, is not possible. Since only one of them can be diagonalised at once, it is not obvious how the six-dimensional integration over *all* entries of the matrix  $\tilde{\zeta}$  can be circumvented.

Furthermore, Eq. (23) is incomplete in the sense that it neglects the constraint that the first derivatives  $\eta$  have to vanish for a maximum. Rossi (2012, 2013) only take into account the Hessian which has to be positive definite (actually, it should be *negative* definite for a maximum) and therefore their probability is not only based on maxima in the density field but also on areas for which the first derivative is non-zero. Equation (6) is more specific in that respect since it takes the constraint  $\eta = 0$  explicitly into account (see also Bardeen et al. 1986).

## 3. Results

In this section, I present some numerical results based on the theoretical work developed in the previous section. For the calculation, I adopt a flat reference  $\Lambda$ CDM model with matter density  $\Omega_m = 0.3$ , dark-energy density  $\Omega_\Lambda = 0.7$ , baryon density  $\Omega_b = 0.04$ , a Hubble constant of  $h = 0.7$  in units of  $100 \text{ km s}^{-1} \text{ Mpc}^{-1}$ , and power spectrum normalisation  $\sigma_8 = 0.8$ . All previous values are set at redshift  $z = 0$ . The primordial spectral index of the power spectrum is set to  $n_s = 1$ , and I adopt the transfer function of Bardeen et al. (1986).

In the following, I compare the distribution (6) with the distribution

$$P(e, p | \tilde{\delta}) = \frac{1125}{\sqrt{10}\pi} e(e^2 - p^2) \tilde{\delta}^5 \exp \left[ -\frac{5}{2} \tilde{\delta}^2 (3e^2 + p^2) \right] \quad (24)$$

(Sheth et al. 2001), which expresses the same probability as Eq. (6) except that the maximum constraint is not taken into account, for different values of

$$v \equiv \delta_c^2 / \sigma_0^2(R). \quad (25)$$



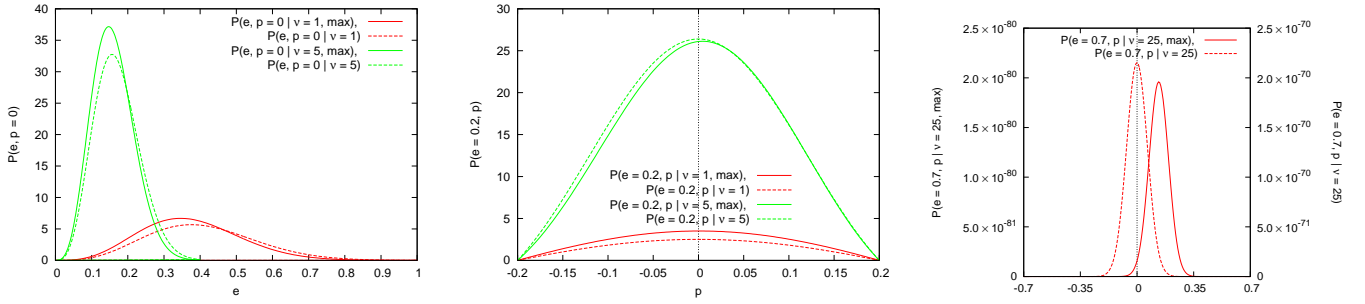


**Fig. 2.** The distributions  $P(e, p | \nu, \text{max})$  and  $P(e, p | \nu)$  for fixed values of either  $e$  or  $p$ . *Left panel:*  $p = 0$  for  $\nu = 1$  and  $\nu = 5$ . *Central panel:*  $e = 0.2$  for  $\nu = 1$  and  $\nu = 5$ . *Right panel:*  $e = 0.7$  for  $\nu = 25$ .

Here,  $\delta_c$  is the linear overdensity of the spherical-collapse model, and  $\sigma_0(R)$  is the power spectrum's variance exponentially filtered on the scale  $R$  (cf. Eq. 3). Hence, for a given  $\nu$ , the radius  $R$  has to be chosen such that Eq. (25) is fulfilled.

In Fig. 1, I compare the distributions (6) and (24) as a function of  $e$  and  $p$  for four different values of  $\nu$ . For each  $\nu$ , the corresponding reduced density contrast is simply  $\delta = \sqrt{\nu}$ . From Eq. (25), one can infer a corresponding filter radius  $R$  that is then used to calculate the higher spectral moments  $\sigma_1(R)$  and  $\sigma_2(R)$  from Eq. (3) and then also  $\gamma(R) = \sigma_1^2(R)/[\sigma_0(R)\sigma_2(R)]$ .

The difference between the two distributions  $P(e, p | \nu, \text{max})$  and  $P(e, p | \nu)$  is the larger the smaller  $\nu$  is. Taking the maximum constraint into account, the distribution for  $e$  and  $p$  peaks at slightly lower values of  $e$ , implying that haloes of lower mass tend to be slightly less elliptical than predicted by the standard formula (24). As a consequence of the normalisation to unity, also the peak's height is larger. However, the higher  $\nu$  is – and therefore the larger a halo's mass is – the more the difference between the two distributions decreases.

The physical reason why the two distributions should be more similar for large values of  $\nu$  instead of small ones is the following. For large  $\nu$ , the Gaussian random field is filtered over a large volume, and maxima at  $\delta = \delta_c$  correspond to maxima whose heights are  $\sqrt{\nu}$  times the standard deviation. The number density of points with  $\nu = 25$  corresponding to  $\delta_c/\sigma_0 = 5$  is fairly small and the probability that such a point is additionally a maximum is fairly high. Hence, the requirement that these points correspond to maxima in the density field is almost always fulfilled naturally and then does not impose an additional constraint. In the limit  $\nu \rightarrow \infty$ , the two distributions should be identical.

In Fig. 2, I present three cuts through the distributions  $P(e, p | \nu, \text{max})$  and  $P(e, p | \nu)$  to highlight the differences between them. The cut at vanishing prolativity shown in the left panel for  $\nu = 1$  and  $\nu = 5$  underlines that the former peaks at lower ellipticity compared to the latter.

The central panel presents a cut at  $e = 0.2$  again for  $\nu = 1$  and  $\nu = 5$ . Contrarily to  $P(e, p | \nu)$ , the distribution  $P(e, p | \nu, \text{max})$  does not peak at  $p = 0$  for a given  $e$  but is shifted towards small positive values for  $p$ , which can be only seen by eye for  $\nu = 5$ .

To stress this additional feature which is not obvious from the 2D distributions in Fig. 1, I present a cut for  $e = 0.7$  at  $\nu = 25$  in the right panel of Fig. 2. At this high value for  $\nu$ , the amplitudes of both distributions are very low ( $\sim 10^{-80}$  for  $P(e, p | \nu, \text{max})$  and  $\sim 10^{-70}$  for  $P(e, p | \nu)$ ) but the asymmetry of the former is now clearly visible: it peaks at  $p \approx 0.13$  instead of 0.

What is most important for practical purposes, however, is not the full distribution for  $e$  and  $p$ , but only the values that are either expected or most probable. The expectation values of  $e$

and  $p$  are used e.g. by Angrick & Bartelmann (2009) to determine the initial eigenvalues for the ellipsoidal-collapse model by Bond & Myers (1996), whereas the most probable values are used by Sheth et al. (2001) to determine the ellipsoidal barrier when establishing their mass function. The expectation values for  $e$  and  $p$  as well as their variances can be calculated analytically for the distribution  $P(e, p | \nu)$ . They are as a function of  $\nu$

$$\begin{aligned} \langle e \rangle &= \frac{3}{\sqrt{10\pi\nu}}, & \sigma_e^2 &= \frac{19\pi - 54}{60\pi\nu}, \\ \langle p \rangle &= 0, & \sigma_p^2 &= \frac{1}{20\nu} \end{aligned} \quad (26)$$

(Angrick & Bartelmann 2009). The most probable values for  $e$  and  $p$  from the same distribution are

$$e^{\text{mp}} = \frac{1}{\sqrt{5\nu}}, \quad p^{\text{mp}} = 0, \quad (27)$$

respectively (Sheth et al. 2001).

In Fig. 3, I present the expectation values for both ellipticity and prolativity as well as their  $1-\sigma$  regions for the two distributions  $P(e, p | \nu, \text{max})$  and  $P(e, p | \nu)$  as a function of  $\nu$ . As expected, the expectation value for the ellipticity is smaller if the maximum constraint is taken into account and the expected prolativity has a small non-vanishing value. For larger  $\nu$ , the difference between both distributions decreases. While the largest difference in  $\langle e \rangle$  is at  $\nu \approx 1.4$  with a value that is  $\sim 8\%$  lower if the minimum constraint is taken into account, the difference in  $\langle p \rangle$  is monotonically decreasing with increasing  $\nu$  and has a value of  $\sim 0.0085$  at  $\nu = 0.1$  and  $\sim 0.005$  at  $\nu = 1.4$ . For  $\nu = 25$ , the difference in  $\langle e \rangle$  has dropped to  $\sim 1.3\%$  and  $\sim 0.00015$  for  $\langle p \rangle$ . At the borders of the  $1-\sigma$  regions, the discrepancy between the results from the two distributions (6) and (24) is of equal magnitude as for the expectation values themselves.

Although  $P(e, p | \nu, \text{max})$  peaks at relatively large values of  $p$  for large  $e$  and  $\nu$  as shown in the right panel of Fig. 2, its amplitude has already fallen off by several orders of magnitude compared to the maximum so that this effect does not have any large influence when calculating the expectation value of  $p$ . Hence,  $\langle p \rangle$  calculated from (6) does in fact approach 0 for  $\nu \rightarrow \infty$  relatively quickly.

In Fig. 4, I compare the most probable values  $e^{\text{mp}}$  and  $p^{\text{mp}}$  from the two distributions with each other. Qualitatively, the dependence on  $\nu$  is like for the most probable values for both ellipticity and prolativity. At  $\nu \approx 1.5$  the relative difference in  $e^{\text{mp}}$  is maximal with a value that is  $\sim 8\%$  lower if the minimum constraint is taken into account. At  $\nu = 25$  the difference has dropped to  $1.4\%$ . The most probable value for  $p$  is  $\sim 0.006$  for  $\nu = 0.1$  and has dropped to  $\sim 0.00005$  for  $\nu = 25$ .

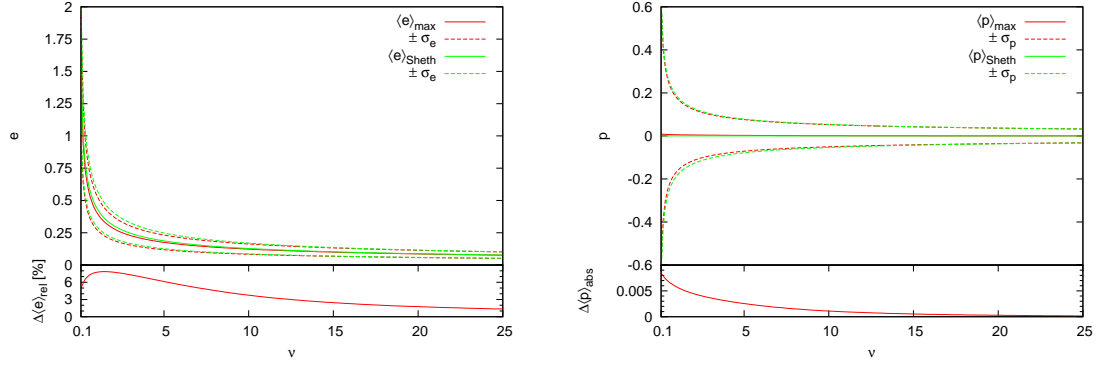


**Fig. 3.** Expectation values for the ellipticity (*left panel*) and the prolativity (*right panel*) as well as their 1- $\sigma$  regions for the two distributions  $P(e, p | \nu, \text{max})$  and  $P(e, p | \nu)$  as a function of  $\nu$ . Quantities derived from the two distributions are denoted by the subscript “max” and “Sheth”, respectively. At the bottom of each plot, the differences between the results from both distributions are quantified. In the left panel, the *relative* difference is given by  $\Delta \langle e \rangle_{\text{rel}} = (\langle e \rangle_{\text{Sheth}} - \langle e \rangle_{\text{max}}) / \langle e \rangle_{\text{Sheth}}$ , whereas in the right panel, the *absolute* difference is simply  $\Delta \langle p \rangle_{\text{abs}} = \langle p \rangle_{\text{max}} - \langle p \rangle_{\text{Sheth}} = \langle p \rangle_{\text{max}}$ .

In summary, the ellipticity used in analytical models of structure formation is about 1 – 8 % too low in the range of  $\nu$  relevant for cosmology since the maximum constraint is not taken into account. The prolativity is usually assumed to vanish, but should be slightly positive with values at the level of  $10^{-5}$  to  $10^{-2}$  in the same range.

#### 4. Summary & conclusions

In this article, I have derived the conditional probability for the gravitational-shear field’s ellipticity and prolativity at the position of a peak in the density field with a given height. The derivation is based on the statistics of Gaussian random fields (Bardeen et al. 1986) and extends the works by Sheth et al. (2001) and Rossi (2012, 2013) as follows. In contrast to Sheth et al. (2001), I have added explicitly the maximum constraint in the calculation since it is expected that haloes form at the positions of peaks in the density field. Although Rossi (2012, 2013) started going into the same direction, they have considered the conditional eigenvalues of the matrix  $\bar{\phi} | \bar{\zeta}$  and the corresponding ellipticity and prolativity constructed from the constrained eigenvalues but not the unconditional ones that serve as ingredients for the ellipsoidal-collapse model by Bond & Myers (1996). Additionally, they only considered that the density’s Hessian has to be negative definite for a maximum but did not take into account that the first derivative  $\eta$  has also to vanish.

The main results of this article can be summarised as follows:

- The gravitational-shear tensor  $\phi$  and the density’s Hessian cannot be diagonalised simultaneously. Since the eigenvalues of  $\phi$  are needed for the definition of the ellipticity  $e$  and prolativity  $p$ , the priority is on the diagonalisation of  $\phi$  so that first, the constraint that the density’s Hessian  $\zeta$  has to be negative definite for a maximum can only be considered via Sylvester’s criterion and second, the full six-dimensional integration over  $d^6\zeta$  has to be carried out.
- The conditional probability for  $e$  and  $p$  given a density maximum of height  $\delta$  is given by (6) after rescaling to  $\tilde{\delta} = \delta/\sigma_0$ . The numerator can be calculated by Eqs. (15) and (16), while the denominator is given by Eqs. (21) and (22). Equation (18) takes into account that one has to integrate Eq. (15) only over those subvolumes for which the Hessian  $\zeta$  is negative definite.

- The distribution of  $e$  and  $p$  incorporating the maximum constraint peaks at lower ellipticities and slightly positive prolativities compared to the unconstrained one by Sheth et al. (2001).
- As a consequence, both the expected and the most probable ellipticity are about 1 – 8 % smaller for  $0.1 \leq \nu \leq 25$  with the largest deviation at around  $\nu \sim 1.4 - 1.5$ . Both the expected and the most probable prolativity have slightly positive values at the level of  $10^{-5}$  to  $10^{-2}$  with increasing value for decreasing  $\nu$ .
- Although the most probable prolativity can have relatively large values for large  $\nu$  and  $e$ , the probability density is several orders of magnitude lower compared to the peak value so that this yields only moderate changes in  $\langle p \rangle$  and  $p^{\text{mp}}$ .
- Both expected and most probable values for ellipticity and prolativity from the distribution  $P(e, p | \nu, \text{max})$  tend to converge to the values from the distribution  $P(e, p | \nu)$  for  $\nu \rightarrow \infty$  since the larger  $\nu$ , the more often is the maximum constraint automatically fulfilled.

The additional maximum constraint alters the main results from the distribution for  $e$  and  $p$  only moderately and especially for small values of  $\nu$ . Massive haloes should therefore be less affected from this conclusion.

However, it will be interesting to see if the slightly positive values for  $\langle p \rangle$  and  $p^{\text{mp}}$  do have an impact on the ellipsoidal-collapse model by Bond & Myers (1996) when using the linear approximation for the external shear since in this model, the eigenvalues of the external shear tensor  $\lambda_{\text{ext},i}$  scale with the linear growth factor of structure formation with time. From the  $P(e, p | \nu)$ , it follows that  $\lambda_{\text{ext},3} = -\lambda_{\text{ext},1}$  and  $\lambda_{\text{ext},2} = 0$  so that  $\lambda_{\text{ext},2} = 0$  stays zero over the whole period of time when the ellipsoid first expands and then collapses. This, however, will change if  $\lambda_{\text{ext},2} \neq 0$  for small times since it will grow over time according to the linear growth factor of structure formation.

*Acknowledgements.* I want to thank M. Bartelmann for carefully reading the manuscript and for the suggestions that helped to improve it and B.M. Schäfer for the discussions that finally led to the implementation of Sylvester’s criterion.

#### References

- Angrick, C. & Bartelmann, M. 2009, A&A, 494, 461  
 Bardeen, J. M., Bond, J. R., Kaiser, N., & Szalay, A. S. 1986, ApJ, 304, 15  
 Bartelmann, M., Ehlers, J., & Schneider, P. 1993, A&A, 280, 351

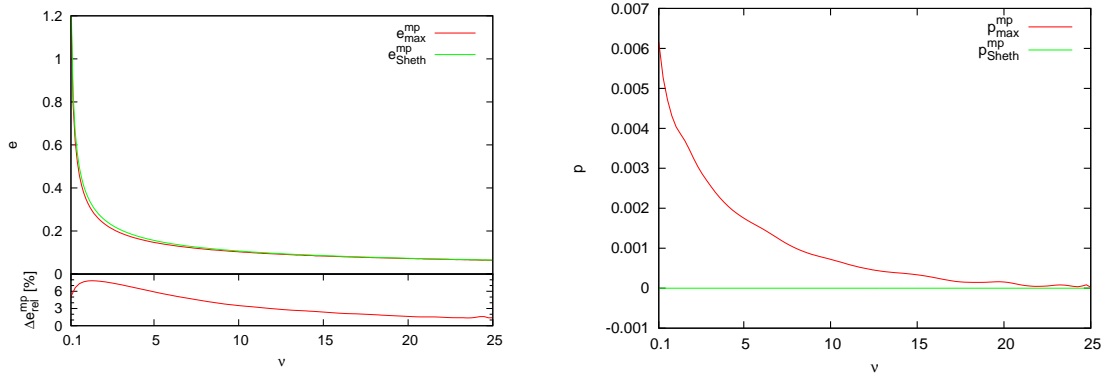


**Fig. 4.** Most probable values for the ellipticity (*left panel*) and the prolaticity (*right panel*) for the two distributions  $P(e, p | \nu, \text{max})$  and  $P(e, p | \nu, \text{Sheth})$  as a function of  $\nu$ . Quantities derived from the two distributions are denoted by the subscript “max” and “Sheth”, respectively. At the bottom of the left plot, the relative difference between the results from both distributions is quantified. Further denotations are as in Fig. 3. (The small bumps in the curves, especially in the right panel, occur from numerical noise.)

- Bond, J. R. & Myers, S. T. 1996, ApJS, 103, 1  
Doroshkevich, A. G. 1970, Astrophysics, 6, 320  
Eisenstein, D. J. & Loeb, A. 1995, ApJ, 439, 520  
Pace, F., Waizmann, J.-C., & Bartelmann, M. 2010, MNRAS, 406, 1865  
Planck Collaboration XXIV. 2013, arXiv:1303.5084  
Rossi, G. 2012, MNRAS, 421, 296  
Rossi, G. 2013, MNRAS, 430, 1486  
Sheth, R. K., Mo, H. J., & Tormen, G. 2001, MNRAS, 323, 1  
Wang, L. & Steinhardt, P. J. 1998, ApJ, 508, 483  
Zel'dovich, Y. B. 1970, A&A, 5, 84